CHAPTER – I

INTRODUCTION

CONTENTS

1.1 INTRODUCTION

Issues pertaining to water contamination becomes of paramount importance due to fundamental role of water in sustaining life. Water constituted a significant portion of the human body (about 70%) and served as a cornerstone of life. The adverse effect of water pollution on human health and environmental integrity deepens the critical nature of water-related concerns. Therefore, an urgent attention is required to find out some solution for pressing need to combat water pollution.

The textile, dyeing, printing industries are largest consumer of fresh water per Kg of treated material. The effluents from these industries contains toxic, carcinogenic, and persistent chemicals such as dyes, formaldehyde, dioxins, heavy metals, etc. Dyes have complex structures and these are degraded naturally at high temperatures in alkaline condition under ultraviolet radiation and with another radical initiator forming toxic by-products, which may be sometimes more toxic to the environment than the parent compound. These dyes are mostly resistant to thermal, chemical, microbial, and photolytic degradation as many of them are recalcitrant in nature. Thus, there is a need of an effective, ecofriendly and economical technique for removing or degrading these dyes from wastewater. Several conventional methods for treating wastewater containing dyes from different industries are used to date, such as photodegradation, adsorption, filtration, coagulation, biological treatments, etc. However, some of these techniques are not much more effective due to the stability of pollutant molecules, and other demerits. Thus, advanced oxidation processes have been reported in oder to degrade such molecules to reduce the load of organic pollutants into wastewater.

1.2 ADVANCED OXIDATION PROCESSES

Advanced oxidation processes are genuinely efficient for treating various toxic organic pollutants and complete destruction of contaminants of emerging concern like naturally occurring toxins, pesticides, dyes, and other deleterious contaminants. These organic pollutants interact with hydroxyl radical via addition or hydrogen abstraction pathways, resulting in a carbon-centered radical, which then reacts with molecular oxygen to form a peroxyl radical that undergoes subsequent reactions; thus, generating a host of oxidation products like ketones, aldehydes, or alcohols. Hydroxyl radicals can

also form a radical cation by abstracting an electron from electron rich substrates, which can readily hydrolyze in aqueous media giving an oxidized product. The oxidation products are often less toxic and more susceptible to bioremediation like CO_2, water, etc.

Advanced oxidation involves these basic steps:

- The first step involves the formation of strong oxidants like $^{\bullet}OH$, $HO_2^{\bullet}$, $O_2^{\bullet-}$, etc.
- In the second step, these oxidants react with organic contaminants presents in the waste water converting them into biodegradable compounds and
- The last step is the oxidation of these biodegradable intermediates leading to complete mineralization in water, carbon dioxide, and inorganic salts.

1.2.1 Types of AOPs

Advanced oxidation processes have mainly these processes.

- UV-Hydrogen Peroxide Processes
- Fenton and Photo-Fenton Processes
- Ferrioxalate-Mediated Processes
- Ozone-Based Processes
- Photocatalysis
- Sonolysis
- Microwave/Hydrogen Peroxide Processes
- Gamma-ray, X-ray and Electron Beam Based Processes
- Supercritical Water Oxidation
- Electrochemical Oxidation Processes
- Catalytic Wet Peroxide Oxidation

1.2.2 Advantages of Advanced Oxidation Processes

- AOP processes can be used to remove or degrade organic pollutants in aqueous medium itself rather than transfer of these pollutants into another phase, such as solid waste.
- The hydroxyl radical reacts with all the non-degradable (recalcitrant) aqueous pollutants, heavy metals, etc., and
- It is commonly used in disinfection.

1.2.3 Limitations of Advanced Oxidation Process

- AOPs involved relatively high capital and maintenance costs.
- A regular addition of some chemical reagents may be required, which may be quite expensive.
- In this procedure, removal of residual peroxide is also to be considered as it can have potential adverse effects on later treatment steps. The residual hydrogen peroxide may be harmful to life.

1.3 PHOTOCATALYSIS

The term photocatalyst is a combination of two words: Photo related to photon and catalyst, which is a substance affecting the reaction rate in its presence. Therefore, photocatalysts may be defined as materials, which can change the rate of a chemical reaction on exposure to light. This phenomenon is known as photocatalysis. The process of photocatalysis includes reactions that take place by utilizing light in presence of a semiconductor. The compound that absorbs light and acts as a catalyst for these chemical reactions is known as a photocatalyst. All such photocatalysts are mostly semiconductors.

The energy difference between the valence band (Highest occupied molecular orbital or HOMO) and the conduction band (Lowest unoccupied molecular orbital or LUMO) is called as the band gap. On the basis of this energy band gap, the materials are classified into three basic categories.

- Metal or Conductor: $E_g < 1.0$ eV
- Semiconductor: $E_g < 1.5$-3.0 eV
- Insulator or Nonconductor: $E_g > 5.0$ eV

These are given diagrammatically in fig. 1.1

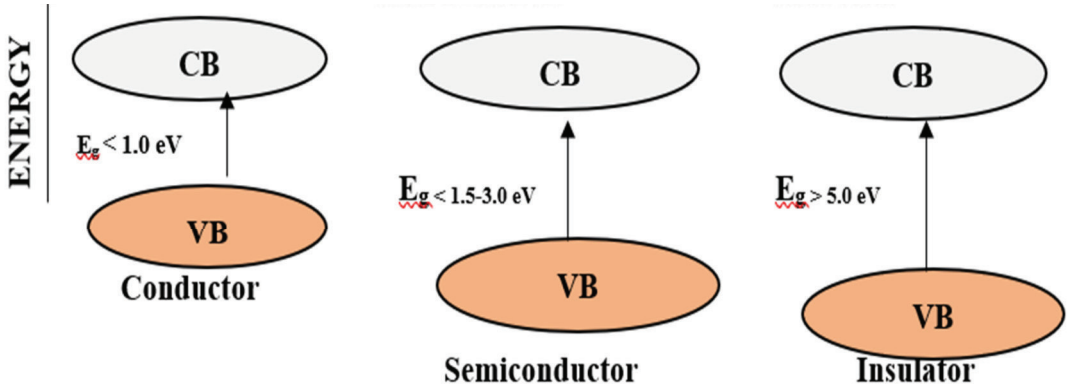

Fig. 1.1 Energy Difference b/w HOMO and LUMO

1.3.1 Types of Photocatalysis

(i) Homogeneous photocatalysis, where substrate and photocatalyst; both exist in the same phases i. e. gas, solid, or liquid, Such photocatalytic reactions are termed as homogeneous photocatalysis. Different dyes and some soluble coordination compounds are used as homogeneous photocatalysts.

(ii) Heterogeneous photocatalysis, in which substrate and photocatalyst exist in different phases. Different semiconducting powders are good examples of heterogeneous photocatalysts. Most of the transition metal chalcogenides are the most common examples of heterogeneous photocatalysts.

1.3.2 Mechanism of photocatalysis

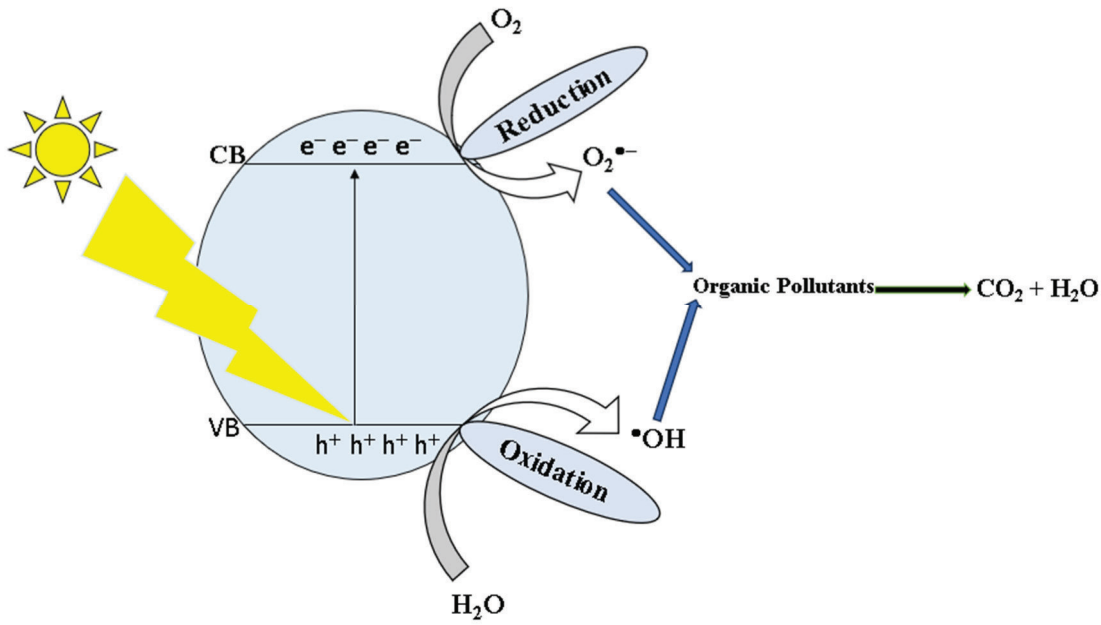

Fig. 1.2 Mechanism of Photocatalysis

Light interacts with the photocatalyst in the process of photocatalysis. When a photocatalyst absorb photon, the e^- present in the valence band is excited to conduction band of the catalyst. As a resultant, electron-hole pair is generated through this photoexcitation. The e^- and hole react with absorbed O_2 and H_2O on the surface of catalyst to from reactive oxidizing species (like $O_2^{\bullet-}$ and $^{\bullet}OH$) that react with the organic pollutants present in water and oxidized it to CO_2 and H_2O through some intermediate steps.

1.3.3 Modification of Photocatalyst

Efficiency of a photocatalyst can be enhanced by:

- Formation of localized state just above the valence band,
- Formation of localized state just below the conduction band,
- Using photocatalyst with low band gap, and
- Color center formation in band gap and surface modification.

Some of the important techniques for modification of photocatalyst are:

- Doping with metal or nonmetal,
- Codoping with various combination of donor and acceptor materials,
- Coupling of photocatalyst, composite formation,
- Sensitization,
- Use of Co-catalyst, and
- Use of heterojunction (Z-scheme and S- scheme).

1.4 PHOTOCATALYTIC DEGRADATION

Bae et al.[1] prepared metal-doped TiO_2 nanoparticles via hydrothermal and sol-gel methods. They used Cr, Co and N-doped TiO_2 for photocatalytic degradation of IPA to CO_2, but it was observed that only Cr-doped TiO_2 could produce H_2 photocatalytically in the presence of methanol-water solution under visible light. It was also revealed that in case of Pt/Co-doped TiO_2, the electron excited to the conduction band has a sufficient reduction potential so as to reduce H^+ ion to hydrogen, but hole present in the valence band has lower oxidation potential than required for degradation of methane to CO_2.

Li et al.[2] prepared tungsten-doped TiO_2/activated carbon catalysts. It was reported that W–TiO_2 layer was coated on the AC surface, which has higher surface area and smaller crystallite size as compared to TiO_2/AC. It was revealed that doping by W is responsible for narrowing the band gap of TiO_2 and as a consequence, its optical response is shifted from the ultraviolet to visible-light region. They evaluated photocatalytic performances of this supported catalyst for degradation of rhodamine B (RhB) under visible-light irradiation. They also investigated effects of tungsten ion content, TiO_2 content, pH, catalyst amount, and initial RhB concentration on degradation of Rh B.

Khairy and Zakaria[3] prepared M-doped TiO_2 nanoparticles (M = Zn, Cu) through sol–gel method. Then they investigated photocatalytic activities of these samples for degradation of methyl orange (MO) and chemical oxygen demand (COD). It was

observed that anatase phase of TiO_2 nanoparticles was formed with crystallite sizes ranging between 9–21 nm. It was observed that doping of ions to TiO_2 lead to an increase in the absorption edge wavelength, and correspondingly, a decrease in the band gap energy of TiO_2 nanoparticles was recorded. It was revealed that Cu doped TiO_2 nanoparticles displayed highest photocatalytic activity as compared to others based on the COD values.

Li et al.[4] synthesized functionalized photocatalyst (Mo- doped WO_3 that is active as well as stable. Here, it was assumed that Mo was homogeneously doped into the crystal lattice of tungsten oxide. It was also revealed that 2D structure of photocatalyst (nanosheet) was beneficial for charge transfer by Mo doping and it changed the band structure of WO_3. As a result, photocatalytic activity of Mo doped WO_3 was improved for degradation of rhodamine B.

Zhang et al.[5] synthesized N-doped mesoporous ZnO nanospheres through solvothermal approach. The photocatalytic activities of as-prepared composites were evaluated for degradation of rhodamine B at room temperature with near-UV light irradiation. It was reported that these nanocomposites exhibited higher photocatalytic activity as compared with pure ZnO nanoparticles. This increase in photocatalytic activity of N-doped ZnO nanoparticles was due to absorption of more photons and reduced electron–hole pair recombination.

Luan et al.[6] prepared Bi_2AlVO_7 and Bi_2InTaO_7 via solid-state reaction. It was reported that band gaps of Bi_2AlVO_7 and Bi_2InTaO_7 were formed to be 2.06 and 2.81 eV, respectively. These catalyst were then used for photocatalytic degradation of methylene blue (MB) dye under visible light irradiation. It was observed that Bi_2AlVO_7 displayed higher photocatalytic activity as compared with Bi_2InTaO_7 for photocatalytic degradation of MB. It was also revealed that complete removal of MB could be achieved in 160 min using Bi_2AlVO_7 as the photocatalyst.

Wahyuni et al.[7] carried out photocatalytic removal of Cu (II), Cd (II), Cr (VI) and Pb (II) with TiO_2 under UV irradiation. The maximum effectiveness of this photocatalytic process was obtained with 50 mg of TiO_2 at pH 5, which can remove 45.56%, 77.72%, 15.23%, and 40.32%, of Cu (II), Cr (VI), Cd (II) and Pb (II), respectively.

Benjwal et al.[8] synthesized reduced graphene oxide (rGO) and metal oxide-based binary (rGO-TiO_2/rGO-Fe_3O_4) and ternary (rGO-Fe_3O_4-TiO_2) nanocomposites in a simple one-step via solvothermal process. It was observed that ferric oxide and titania nanoparticles were firmly anchored over rGO. Then they used as-synthesized nanocomposites for the removal of methylene blue dye under UV as well as visible light irradiations. Ternary (rGO-Fe_3O_4-TiO_2) nanocomposite exhibited the highest dye degradation efficiency (almost 100%) within 5 min as compared to binary nanocomposite.

Das et al.[9] synthesized manganese (III) acetylacetonate complex [Mn $(acac)_3$] over graphitic carbon nitride (GCN), (2-Mn/GCN) via ultrasonication method. This as-prepared 2-Mn/GCN could achieve 99.59% degradation of rhodamine B in 55 min and 97.6% metronidazole (MTZ) was degraded in 40 min, when 0.7% Mn content was there in the catalyst.

Akhundi and Habibi Yangjeh[10] decorated $CuCr_2O_4$ nanoparticles on to g-C_3N_4 nanosheets (g-C_3N_4-NS) through reflux. The photocatalytic performance of g-C_3N_4-NS/$CuCr_2O_4$ nanocomposites was evaluated for degradation of methylene blue, rhodamine B and phenol under visible-light irradiation. When the loading amount of $CuCr_2O_4$ was 10 wt%. The nanocomposite exhibited the highest activity. Activity of the g-C_3N_4-NS/$CuCr_2O_4$ (10%) nanocomposite refluxed for 3 h and calcined at 520 °C for 4 h was almost 11.8 and 4.8 times greater than those of the bulk g-C_3N_4 and g-C_3N_4-NS photocatalysts in degradation of RhB, respectively. In the prepared nanocomposites, nanosheets of g-C_3N_4 act not only as $CuCr_2O_4$ support, but also as co-catalyst. The novel visible-light-active photocatalyst has considerable stability and it can be reused for five times without obvious loss of its photocatalytic activity.

Dahiya et al.[11] synthesized Ag-doped graphitic carbon nitride (AgGCN). The silver nanoparticles, were prepared using leaf extract of the *Ocimum tenuiflorum* (Tulsi) served as a stabilizing as well as capping agent. Different concentrations of the prepared series of nanocomposites Ag-doped GCN (0.5 mM, 1.0 mM, 1.5 mM, and 2.0 mM) were used for photocatalytic degradation of xylenol orange (XO) and rose Bengal (RB) dyes. It was observed that degradation efficiency increased due to the doping of Ag nanoparticles into GCN from 15 to 36% and 54 to 76% in the case of RB and XO,

respectively. It was also revealed that rate constant increased up to 2.5 times when Ag-doped GCN (1.5 mM) nanocomposite was used as compared to GCN.

Parthipan et al.[12] used hydrothermal route to synthesize reduced graphene oxide (PErGO) using *Phyllanthus emblica* fruits extract. The photocatalytic removal of methylene blue (MB) and methyl orange (MO) was investigated in presence of PErGO, and it was observed that about 92 and 91% MO and MB was degraded within 90 min of sunlight exposure, when mixed dye degradation was carried out. The stability and reusability of this catalyst was confirmed and it was revealed that it can be used for five degradation cycles without any significant degradation in its activity.

Gogoi et al.[13] prepared graphene oxide–clay nanocomposite. As-prepared graphene oxide-clay nanocomposite was then used for photodegradation of methylene blue. It was observed that as-prepared nanocomposite was found active against cationic dye, but it was not effective against degradation of other anionic dyes Eosin yellow and methyl orange. It was also evaluated for its reuse and it was found that percentage degradation was 85, 75 and 75 for first, second and third cycles, respectively.

Jin et al.[14] reduced GO to reduced graphene oxide (rGO) by *Eucalyptus* leaf (EL) extract. Results confirmed the oxygen-containing groups in GO were efficiently removed, formation of capping layer on the surface of rGO, and good dispersion of rGO in aqueous solution. The removal of methyl blue (MB) on EL-rGO, activated carbon, graphite powder and commercial graphene was investigated and maximum adsorption capacity of different adsorbents followed the order:

EL-rGO > Commercial graphene > Activated carbon > Graphite powder.

Yuan et al.[15] used potassium ion-doped precursor, potassium sorbate, in melamine configuration during calcination to prepare the potassium-doped g-C_3N_4 (KCN). It was reported that doping of potassium in g- C_3N_4 can modify the band structure so that light absorption and photogenerated carrier separation was enhanced. It was then used for photodegradation of methylene blue (MB).

Kuo et al.[16] modified the surface of Degussa P25 TiO_2 to prepare phosphorus-doped TiO_2 (P-TiO_2). Then they evaluated photocatalytic activity of TiO_2 and P-TiO_2 for

the degradation of bisphenol A (BPA) under UV and sunlight irradiation both. It was reported that band gap of TiO_2 and P-TiO_2 was 3.1 and 3.0 eV, respectively. It was revealed that degradation of BPA by the UV/TiO_2, UV/P-TiO_2, sunlight/TiO_2 and sunlight/P-TiO_2 systems was 59, 65, 84 and 92 % respectively. This degradation obeyed pseudo-first order kinetics. The higher degradation of BPA was attributed to narrowed band gap, reduced recombination of photogenerated electrons and holes and increased number of hydroxyl groups on surfaces.

Pham et al.[17] synthesized graphitic carbon nitride (g-CN), (metal-free photocatalyst) by polymerizing melamine and used it for photodegradation of carbamazepine (CZ) and acetaminophen (AP) in wastewater. It was reported that high removal efficiencies of 89.5% and 98.6% could be obtained for CZ and AP respectively. The rate of photodegradation with synthesized photocatalyst was 0.0321 min^{-1}, which was 2.14 times faster than in case of CZ. It was also revealed that g-CN was active under solar light because it generated highly reactive oxidants such as superoxide ($^{\bullet}O_2^-$) and hydroxyl ($^{\bullet}OH$) radical. The stability of g-CN for treating these pharmaceuticals was also ascertained by using it for three repeated cycles.

Al-Zahrani et al.[18] prepared graphitic carbon nitride (g-C_3N_4) utilized it for photocatalytic degradation of acid red 26 on exposure to UV-A light. It was reported that photocatalytic degradation of acid red 26 involved dealkylation, oxidation, and cleavage of methoxy group The role of reactive species h^+ and $O_2^{\bullet}$ in this degradation process was ascertained byscavengers studies.

Binary metal oxides have also been widely used as photocatalysts for decades because the morphological properties of the individual oxides can be changed by formation of new sites in the interface between the components, or by incorporation of one oxide into the lattice of the other.

Ben et al.[19] synthesized graphitic carbon nitride–bismuth phosphate nanocomposite ($BiPO_4$ g-C_3N_4). It was reported that azo dyes such as reactive red 120 raise great concerns about their increased harmfulness. Photocatalytic degradation is considered to be one of the most efficient techniques for reactive red 120 degradation. The band gap energies of the, $BiPO_4$, g-C_3N_4 and $BiPO_4$ g-C_3N_4 nanocomposite were calculated as 4.20, 2.66, and 2.68 eV, respectively. It was reported that $BiPO_4$ g-C_3N_4

nanocomposite exhibited higher photocatalytic activity towards the degradation of reactive red 120 (RR120) under sunlight. The reaction rate constant of this degradation was found to be seven and four times higher than $BiPO_4$ nanorods and g-C_3N_4 (0.0036 min^{-1}), respectively. It was revealed that catalyst performance was decreased by less than 5% even after five recycles indicated high stability of this nanocomposite.

Dobrosz-Gomez et al.[20] examined photocatalytic degradation of phenol using TiO_2 loaded with some transition metal ions (Co, Cu, Fe and Mo) under both UV; and visible light. It was reported that most efficient one was Mo/TiO_2. It was indicated that Mo made its surface more acidic. It was observed that percentage of degradation of phenol under visible light was relatively lower than under UV radiation. Out of series of prepared catalysts, 2 wt% Mo/TiO_2 was found to be the most efficient one.

Lei et al.[21] prepared highly active CuO-modified TiO_2 photocatalysts via impregnation method. The CuO/TiO_2 was then used for degradation of polybrominated diphenyl ethers. It was reported that photo-reductive degradation of 2,2′,4,4′-tetrabromodiphenyl ether (BDE47) was almost impossible on TiO_2, but it became rapid on CuO/TiO_2 with an short induction time period (20 s). They proposed "switching reduction potential by the valence state of copper" concept in their mechanism.

Xie et al.[22] prepared a series of α-Fe_2O_3/ZnO composites with different α-Fe_2O_3 contents. The photocatalytic activity of as-prepared composites was evaluated in degradation of pentachlorophenol (PCP). It was reported that composites exhibited higher photocatalytic activity under UV–vis light irradiation as compared to ZnO. The pentachlorophenol was almost completely degraded by this composite within 4 h, when molar ratio was kept 1:5.

Sherly et al.[23] prepared nanostructured ZnO and CuO, and coupled oxides, in different molar ratios (1:1, 2:1, and 1:2). It was reported that optical absorption of ZnO was extended into the visible region on loading of CuO. The photocatalytic activities of ZnO, CuO, and ZnO:CuO were evaluated for photodegradation of 2,4-dichlorophenol under visible light irradiation. It was found that coupled metal oxide exhibited higher photocatalytic activity and it was attributed to the extended photo responsive range and charge separation rate in the nanocomposite.

Vignesh et al.[24] sensitized nanoparticles of zinc oxide (ZnO) with silver iodide. It was reported that average crystallite size of nanoparticles was 21.56 and 23.44 nm for ZnO and AgI sensitized ZnO, respectively. The photocatalytic efficiency of AgI-ZnO was observed for decolorization of rosaniline hydrochloride under visible light irradiation. The effect of different operational parameters on degradation was investigated such as pH, catalyst dosage and dye concentration. It was also revealed that maximum decolorization, total organic carbon (TOC) reduction and COD removal were 88, 75 and 68%, respectively under the optimal conditions.

They also synthesized TiO_2–metal vanadate nanocomposites (TiO_2–MV).[25] The photocatalytic activity of as-prepared TiO_2–MV was evaluated for degradation of fast green (FG) under visible light irradiation. It was reported that photocatalytic activity of as-prepared TiO_2–silver vanadate (TiO_2–Ag_3VO_4) was much higher as-compared to all; TiO_2–cadmium vanadate (TiO_2–CdV_2O_6), TiO_2–strontium vanadate (TiO_2–$Sr_3(VO_4)_2$) and TiO_2. The mineralization of fast green was confirmed by chemical oxygen demand (COD) and total organic carbon (TOC) measurements. It was also revealed that TiO_2–Ag_3VO_4 is a reusable photocatalyst.

Karunakara and Senthilvelan[26] observed photocatalyzed oxidation of aniline to azobenzene in presence of ZrO_2 under natural sunlight and UV irradiation (365 nm). It was reported that electron donors such as hydroquinone, triphenylphosphine and diphenylamine enhanced the photocatalysis. It was also revealed that many oxides like TiO_2, V_2O_5, ZnO, Fe_2O_3, CdO, CdS and Al_2O_3 also photocatalyzed the oxidation of aniline to azobenzene with UV light (254 nm) but ZrO_2 was more efficient than all other photocatalysts. The photocatalytic activities of these oxides followed the order:

$$ZrO_2 > ZnO > V_2O_5 > Fe_2O_3 > CdS > Al_2O_3 > CdO > TiO_2.$$

Vinodgopal et al.[27] used nanostructured semiconductor films of SnO2, TiO2, and SnO2/TiO2 and used for photocatalytic degradation of naphthol blue black (NBB). It was reported that degradation rate was significantly higher for SnO2/TiO2 composite films as compared to SnO_2 and TiO_2 films only. This increased degradation rate was attributed to charge separation.

Fabiyi and Skelton[28] used TiO_2 coated buoyant polystyrene beads for photocatalyzed mineralization of methylene blue. These coated beads exhibited high mechanical stability and also significant photocatalytic activity. It was also revealed by thermogravimetric analysis that these beads had no destructive degradation during photocatalytic process. The catalyst activity also remained high for up to 10 successive runs.

Sivalingam et al.[29] prepared anatase phase titania via solution combustion approach with 156 m^2g^{-1} surface area. It was found that average particle size was 8–10 nm. This as-prepared catalyst was then used for photocatalytic degradation of different dyes (Methylene blue, alizarin S, congo red, methyl red and orange G). The effect of various parameter was investigated such as pH, catalyst loading, initial concentrations of the dyes and transition metal doping. It was observed that an adverse effect on the photocatalytic activity. But this inhibition effect was not observed with Pt impregnated TiO_2.

Tan et al.[30] reported that nanosizing of g-C_3N_4 can improve this photocatalytic property. It was also revealed that H_2 evolution performance in the presence of nanosized g-C_3N_4 was 10.8 times higher than that of bulk g-C_3N_4. This improvement was attributed to photoinduced electron-hole separation and photocatalytic efficiency.

Zeng et al.[31] prepared one-dimensional porous architectural g-C_3N_4 nanorods by direct calcination of hydrous melamine nanofibers. It was reported that oxygen atoms were also doped into g-C_3N_4 matrix, which disturbed the symmetry of pristine g-C_3N_4, and as a result, more effective separation of electron/hole pairs could be achieved. It was observed that oxygen-doped g-C_3N_4 nanorods loaded with Pt exhibited excellent visible-light assisted photocatalytic hydrogen evolution (732 μmol g^{-1} h^{-1}) in the triethanolamine solution and also overall water splitting (29.6 μmol g^{-1} h^{-1}). It was also revealed that removal efficiency of 100% of 2, 4-dinitrophenol degradation could be achieved with for O-doped g-C_3N_4 nanorod within 75 min. They also reported visible-light photocatalytic H_2 evolution (96 μmol g^{-1} h^{-1}) along with 2,4-dinitrophenol degradation in presence of Pt g-C_3N_4 nanorods.

Li et al.[32] synthesized g-C_3N_4/TiO_2 hybrid photocatalysts via modified sol–gel technique using different weight ratio of g-C_3N_4. It was observed that heterojunction was formed between g-C_3N_4 and TiO_2 nanoparticles were well dispersed on g-C_3N_4 sheets. Out of as-synthesized hybrid photocatalysts, g-C_3N_4/TiO_2-80% sample displayed highest photocatalytic degradation of methylene blue under visible light irradiation which was around 3.5 times high as compared to pure g-C_3N_4. This increased activity of g-C_3N_4/TiO_2 hybrid photocatalysts was attributed to the effective separation of photogenerated electron–hole pairs and higher absorption capacity. It was also revealed that these photocatalysts exhibited more stability in photocatalytic performance even after five cycles.

Christoforidis et al.[33] prepared hybrid organic/inorganic nanocomposites containg nanosized iron oxide (metastable β-phase) and graphitic carbon nitride (g-C_3N_4). They also evaluated their photocatalytic activity for photodegradation of rhodamine B, methyl orange (MO), and phenol under simulated solar light and visible light irradiation. This improved photoactivity was attributed to improved optical properties, (narrower band-gap), increased visible light absorption efficiency, and efficient separation of the photoinduced charge carriers due to matched band edges in the heterostructure.

Hong et al.[34] synthesized *in situ* sulfur-doped mesoporous g-C_3N_4 (mpgCNS) using thiourea, with SiO_2 nanoparticles as the hard template. It was reported that mpgCNS had a high surface area of 128 $m^2\ g^{-1}$ with mesopores in the range of 10–20 nm. A downshift of 0.25 eV was observed in its conduction band, when carbon is substituted in mpgCNS. It was also revealed that as-prepared mpgCNS was 30 times more active than g-C_3N_4 in evolution of hydrogen from photocatalytic splitting of water.

Bian et al.[35] synthesized S-doped g-C_3N_4 with a hollow microsphere composition (SCNHM) by S doping. This as-prepared SCNHM had high specific surface area (~81 $m^2\ g^{-1}$). It was reported that SCNHM exhibited higher photocatalytic activity for degradation of tetracycline hydrochloride (TC) as compared to CN, SCN and CNHM samples. It was observed that this photocatalyst could eliminate high-concentration of TC (50 mg L^{-1}) in 18 min and removal efficiencies of 100 mg L^{-1} and 200 mg L^{-1} could reach 92 and 60 % in 30 min.

Gao et al.[36] prepared Bi-doped graphitic carbon nitride nanotubes (BCN nanotubes) with a porous structure by polymerizing a mixture of urea, melamine and bismuth nitrate (pentahydrate). It was reported that this as-prepared BCN nanotubes exhibited excellent photocatalytic activity for the degradation of rhodamine (Rh) B, which was 26.8-fold higher than that with PCN under visible light irradiation.

Xie et al.[37] prepared graphite carbon nitride (GCN)/La_2O_3 (CN/La) via a hydrothermal route. The photocatalytic performance of CN/La-x% photocatalysts was observed for degradation of rhodamine B (RhB), methyl orange (MO), methylene blue (MB) under visible light irradiation. It was reported that optimal photodegradation of 66.6, 99.5 and 100% of MO, Rh B and MB could be achieved in 2 h.

Hadadi et al.[38] prepared a composite of g-C_3N_4 with cadmium selenide with four different CdSe mass loadings (1, 2.5, 5, and 10%). It was reported that modified band structure in this nanocomposite not only improved the visible light absorption, but it also retarded the recombination of photo-induced charge carriers. The photocatalytic degradation of methylene blue (MB) and rhodamine B (RhB) was invastigated under visible light. It was observed that highest degradation rate constant was 0.0222 min^{-1} and 0.0178 min^{-1} for MB and RhB, respectively when g-C_3N_4/CdSe nanocomposite was used with 2.5% CdSe mass content.

Chen et al.[39] prepared double Z-type ternary composite long-after glow/graphitic carbon nitride metal–organic framework ($SrAl_2O_4:Eu^{2+}$, Dy^{3+}/g-C_3N_4/NH_2-UiO-66, SGN) via solvothermal method. They used this as a photocatalyst for removal of methylene blue (MB). It was reported that after 30 min of photocatalytic degradation ratio of SGN was found to be 5.86, 4.04 and 10 times more as compared to long-after glow (SAO), g-C_3N_4 and NH_2-UiO-66, respectively. This high photocatalytic activity of the SGN was attributed to double Z-type electron transfer mechanism. It was also revealed that degradation ratio with ternary SGN was about 50 % after 5 h even in the dark. Superoxide anion radical ($^{\cdot}O_2^-$) was identified to be main active species by quenching experiments.

Ahmed et al.[40] prepared La-$CuFe_2O_4$/g-C_3N_4 (LCFO/CN). The photodegradation efficiency of as-prepared LCFO/CN photocatalyst was investigated for removal of rhodamine B (RhB). An excellent photodegradation (97.35 %) was reported by LCFO/CN-2 heterojunction photocatalyst compared to

LCFO/CN-1 (83.14 %), LCFO (67.13 %), and CFO (62.73 %), respectively, The optimal conditions were observed as: (pH = 6.0, [catalyst] = 0.4 gL^{-1}, [RhB] = 30 mg L^{-1}, and T = 25 ± 1 °C). It was also confirmed that the photostability and reusability of the photocatalyst LCFO/CN-2 nanocomposite was good and can it be reused for five successive cycles.

Sousani et al.[41] synthesized $Ni_{0.8}Co_{0.2}/Zn_{0.8}Cd_{0.2}S$ (ZCS)/g-C_3N_4 (CN) ternary nano-photocatalyst through chemical reduction and hydrothermal methods. Photocatalytic degradation of methylene blue (MB) was carried out under LED lamp (100 W, 400–700 nm) irradiation for 3 h. It was observed that high (85%) degradation efficiency of MB could be achieved within 3 h.

Nivetha et al.[42] prepared g-C_3N_4@$BiTiO_2$/NiO heterostructure photocatalyst and used it for degradation of tetracycline (TC) under visible-light radiation. It was reported that g-C_3N_4@$BiTiO_2$/NiO heterostructure photocatalyst exhibited higher light absorption capabilities due to incorporation of g-C_3N_4 in $BiTiO_2$. It was observed that removal efficiency of 91.2% TC could be achieved within 50 min under visible-light radiation. It was also revealed that $O_2^{\bullet-}$ and $^{\bullet}OH$ radicals are the main active oxidizing species in the degradation process as evident from scavenger studies.

Kumawat et al.[43] investigated the photocatalytic activity of iron zinc cuprate for photodegradation of basic fuchsin under visible light. This photocatalyst $FeZn_2Cu_3O_{6.5}$ was synthesized by the ceramic technique. The progress of the degradation was monitored spectrophotometrically at 544 nm. The optimum rate was observed as: Concentration of basic fuchsin = 1.2×10^{-5} M, pH = 6.0, amount of $FeZn_2Cu_3O_{6.5}$ = 0.10 g and light intensity = 50.0 m Wcm^{-2}.

Abbasi-Asl et al.[44] prepared magnetic $Fe_3O_4/Ag_2C_2O_4/Ag_3PO_4$/Ag nanocomposite via co-precipitation method using *calendula officinalis* seed extract as a stabilizer. This as-prepared quaternary photocatalyst was used for degrading herbicide paraquat (PQ) and food dye brilliant blue FCF (BB) under visible light irradiation. It was reported that degradation efficiency of PQ and BB was found to be 92.72 and 88.9%, respectively under optimal conditions.

Akhundi and Habibi-Yangjeh[45] fabricated g-C_3N_4/Fe_3O_4/Ag/Ag_2SO_3 nanocomposites. It was observed that Ag/Ag_2SO_3 nanoparticles were anchored on to surface of g-C_3N_4/Fe_3O_4 nanocomposite, which is reflected in strong absorption in the visible region. The photocatalytic activity of this nanocomposite was evaluated for degradation of rhodamine B as (40%), which was higher as compared with g-C_3N_4 and g-C_3N_4/Fe_3O_4 by factors of 11.7 and 9.3, respectively. The trapping experiments confirmed that superoxide ion radical was the main active species in the photocatalytic degradation process. It was also revealed that this photocatalyst was reusable for five consecutive cycles.

Qarajehdaghi et al.[46] synthesized carboxymethyl cellulose (CMC) based nanocomposite containing CdS, g-C_3N_4, and rGO (CdS/g-C_3N_4/rGO/CMC). They could achieve 81.93 and 68.87%, removal efficiency of Ciprofloxacin (CIP) and TOC, respectively under optimal conditions as: pH 6.1, 8 mg L^{-1} CIP, and 0.6 g L^{-1} catalyst within 35 min.

Gogoi et al.[47] synthesized Ag/Ag_3PO_4–BiOBr–C_3N_4-1and tuned the band gap to 0.56 eV by variation of amount of C_3N_4. The degradation of reactive red (RR 120) was observed in the presence of this composite under visible-light illumination. It was reported that as-prepared composite exhibited 92.6% degradation efficiency of dye with the removal rate as 0.042 min^{-1}, which was about 5.2, 2.7 and 2.5 times more as compared to Ag/Ag_3PO_4, BiOBr and C_3N_4 particles, respectively. The holes, superoxide and hydroxyl radicals were considered responsible for such degradation. It was also revealed that high stability of this photocatalyst was maintained up to four consecutive cycles.

Hasija et al.[48] fabricated carbon quantum data (CQDs) using naturally occurring bamboo leaves as precursors. As-prepared CQDs were then used for construction of Z-scheme P-doped g-C_3N_4/AgI/ZnO/CQDs (PGCN) heterojunction and degradation of 2, 4-dinitrophenol (DNP). It was reported that synergistic effetct of adsorption and photocatalysis was effective for complete mineralization of DNP into H_2O, CO_2 and inorganic ions. It was interesting to note that as-prepared Z-scheme photocatalyst exhibited stability and recyclability for ten consecutive cycles.

Kumar et al.[49] prepared magnetic quaternary BiOCl/g-C_3N_4/Cu_2O/Fe_3O_4 (BGC-F) nano-heterojunction. Its photodegradation activity for degradation of sulfamethoxazole (SME) was evaluated It was reported that about 99.5% of SME (100 μM) could be degraded in 1 h under visible (Xe) lamp and 92.1% in 2 h under natural sunlight. The activity of this quaternary sample was found to be 7.2, 6.8 and 4.2-folds higher than that of C_3N_4/BiOCl/Fe_3O_4, Cu_2O/BiOCl/Fe_3O_4 and Cu_2O/BiOCl/C_3N_4 junctions, respectively. The major oxidizing species were identified as $O_2^{\bullet-}$ and $^{\bullet}OH$ radicals by scavenging experiments. It was also revealed that 41.6% total organic carbon (TOC) removal was there in 3 h under Xe lamp exposure.

Mousavi et al.[50] synthesized g-C_3N_4/Fe_3O_4/Ag_3PO_4/AgCl nanocomposites via ultrasonic- irradiation method. The photocatalytic activity of this composite was evaluated for degradation of fuchsine, rhodamine B, methyl orange, and phenol under visible-light irradiation It was reported that as-prepared g-C_3N_4/Fe_3O_4/Ag_3PO_4/AgCl (30%) nanocomposite exhibited the highest photocatalytic activity. It was observed that activity of this nanocomposite in degradation of rhodamine B was about 22, 6, and 7.5-times higher as compared to g-C_3N_4, g-C_3N_4/Fe_3O_4/Ag_3PO_4 (20%), and g-C_3N_4/Fe_3O_4/AgCl (30%) samples, respectively. It was also revealed that holes were main active oxidizing species based on trapping experiments.

Wang et al.[51] prepared graphitic carbon nitride (g-C_3N_4) and niobium pentoxide nanofibers (Nb_2O_5 NFs) heterojunction. It was confirmed that Nb_2O_5 NFs were tightly attached onto g- C_3N_4 nanosheets in this g- C_3N_4 / Nb_2O_5 heterojunction. It was reported that as-prepared g- C_3N_4 /Nb_2O_5 heterojunction displayed enhanced photocatalytic activity for degradation of phenol and rhodamine B under visible light irradiation as compared to g- C_3N_4 and Nb_2O_5 NFs. The higher catalytic activity was attributed to mainly synergistic effect between g- C_3N_4 sheets and Nb_2O_5 NFs, which promoted the transferring of carriers, but prohibited recombination, of these carriers. It was also revealed that superoxide radical anion and hole were the major active oxidizing as evident from trapping experiments.

Sahu et al.[52] synthesized polymeric oxygen rich exfoliated graphitic carbon nitride (exfoliated GCN, EGCN) It was reported that as-prepared photocatalyst can be used for photocatalytic degradation of bisphenol A (BPA), which could reach to 99%.

Guo et al.[53] synthesized porous thin g-C_3N_4 nanosheets. It was reported that as-prepared photocatalyst can effectively degrade 99.3% of rhodamine B within 15 min under visible light irradiation which was 16.8 times more than bulk g-C_3N_4. It was also confirmed that stronger oxidizability of holes is responsible for its higher photocatalytic activity.

Habib et al.[54] synthesized graphitic nitride (GN) and its derived polyimides using three different dianhydrides. These as-synthesized photocatalyst were tested for degradation of methylene blue (MB) under light irradiation. It was observed that high photocatalytic performance (96% degradation efficiency) could be achieved in 1 h. This better activity was attributed to an improved degree of crystallinity, appropriate porosity, greater charge separation and high quaternary nitrogen content in spite of lower surface area of polyimide, GN-FDA (6.78 $m^2\ g^{-1}$).

Lyu et al.[55] reported preparation of carbon nitride compounds (CN) complexed on the surface of $CuAlO_2$ substrate (CN-Cu (II)-$CuAlO_2$). It was reported that it exhibited very high activity and efficiency for the degradation of bisphenol-A in water through a Fenton-like process. It was observed that removal of bisphenol A was about 25 times higher as compared to $CuAlO_2$. It was observed that Cu (II) generated on the surface of $CuAlO_2$ resulted in significant decrease of surface oxygen vacancies. It was also revealed that in Fenton-like reactions, electron-rich center around Cu was responsible for the efficient reduction of hydrogen peroxide into hydroxyl radicals. This resulted in excellent catalytic performance for degradation of refractory pollutants.

Jin et al.[56] fabricated MoS_2/Ag/g-C_3N_4 (MS/A/CN) Z-scheme composite with a combined strategy by coupling of MoS_2 and Ag deposition on g-C_3N_4 nanosheets. It was reported that this as-prepared MS/A/CN composite can be used for photocatalytic degradation of tetracycline (TC) with peroxomonosulphate (PMS) under visible light irradiation. This MS/A/CN/PMS system displayed excellent degradation of tetracycline (about 98.9%) in 50 min. This may be due to the synergistic effect of photocatalysis and PMS activation.

Li et al.[57] used Fe-doped g-C_3N_4/graphene (rGO) composite catalysts for activation of peroxymonosulfate (PMS) and degradation of trimethoprim (TMP) under visible light irradiation. It was reported that recombination of photogenerated electron-

hole pairs in graphitic carbon nitride may be suppressed by doping it with Fe and incorporation of reduced graphene oxide (rGO). It was reported that degradation of TMP in presence of 0.2% Fe-g-C_3N_4/2 wt% rGO/PMS was 3.8 times higher than with g-C_3N_4/PMS. It was revealed that degradation efficiency was improved from 61.4% at pH = 3 to nearly 100%. It was also reported that eight intermediates were there, which were derived from demethoxylation, hydroxylation, and carbonylation.

Wang et al.[58] prepared a heterogeneous Co-based catalyst by introducing cobalt species to the cavities of *g*-C_3N_4 through Co-N bonds via calcination and impregnation. Then it was applied for activation of PMS for the degradation of organic contaminates under visible light. It was observed that optimum Co loading was 1.0% in weight, which could degrade rhodamine B completely in 25 min with a 70.5% of total organic carbon (TOC) removal.

Although, number of techniques are available for the treatment of waste water, but majority of them have some or other disadvantages. Therefore, search of a green chemical method for such a treatment seems necessary.

Advanced oxidation processes (AOPs) have been advocated as green chemical pathways in achieving this goal. Out of these AOPs, photocatalysis has emerged as a promising candidate for degradation of most of the organic pollutants.

❐❐❐

REFERENCES

1. S.W. Bae, P.H. Borse, S.J. Hong, J.S. Jang, and J.S. Lee, Photophysical properties of nanosized metal-doped TiO_2 photocatalyst working under visible light, J. Korean Phys. Soc., **51**, S22-S26 (2007). doi:10.3938/jkps.51.22.

2. Y. Li, X. Zhou, W. Chen, L. Li, M. Zen, and S. Qin, Photo decolorization of Rhodamine B on tungsten-doped TiO_2/activated carbon under visible-light irradiation, J. Hazard. Mater., **227-228**, 25-33 (2012). doi: org/10.1016/j.jhazmat.2012.04.071.

3. M. Khairy and W. Zakaria, Effect of metal-doping of TiO_2 nanoparticles on their photocatalytic activities toward removal of organic dyes, Egypt. J. Pet., **23**, 419-426 (2014). doi:10.1016/j.ejpe.2014.09.010.

4. N. Li, H. Teng, Li. Zhang, J. Zhou, and M. Liu, Synthesis of Mo-doped WO_3 nanosheets with enhanced visible-light-driven photocatalytic properties, RSC Advances., **5**, 95394-95400 (2015). doi:10.1039/C5RA17098B.

5. D. Zhang, J. Gong, J.J. Ma, G. Han, and Z. Tong, A facile method for synthesis of N-doped ZnO mesoporous nanospheres and enhanced photocatalytic activity, Dalton Trans., **42**, 16556-16561 (2013). doi.org/10.1039/C3DT52039K.

6. J. Luan, W. Zhao, J. Feng, H. Cai, Z. Zheng, B. Pan, X. Wu, Z. Zou, and Y. Li, Structural, photophysical and photocatalytic properties of novel Bi_2AlVO_7, J. Hazard. Mater., **164**(2–3),781–789 (2009). doi.org/10.1016/j.jhazmat.2008.08.088.

7. E. Wahyuni, N. Aprilita, H. Hatimah, A. Wulandari, and M. Mudasir. Wahyuni, Removal of toxic metal ions in water by photocatalytic method, Am. Chem. Sci. J., **5**(2),194–201 (2015). doi:10.9734/acsj/2015/13807.

8. P. Benjwal, M. Kumar, P. Chamoli, and K.K. Kar, Enhanced photocatalytic degradation of methylene blue and adsorption of arsenic (III) by reduced graphene oxide (rGo)–metal oxide (TiO_2/Fe_3O_4) based nanocomposites, RSC Adv., **5**(89), 73249–73260 (2015). doi:10.1039/c5ra13689j.

9. B. Das, M. Devi, S. Deb, and S. Dhar, Boosting photocatalytic property of graphitic carbon nitride with metal complex fabrication for efficient degradation of organic pollutants, Chemosphere., **323**, (2023). doi: 10.1016/j.chemosphere.2023.138230.

10. A. Akhundi and A. Habibi-Yangjeh, Graphitic carbon nitride nanosheets decorated with $CuCr_2O_4$ nanoparticles: Novel photocatalysts with high performances in visible light degradation of water pollutants, J. Colloid Interface Sci., **504**, 697–710 (2017). doi: 10.1016/j.jcis.2017.06.025.

11. S. Dahiya, A. Sharma, and S. Chaudhary, Synthesis of phytoextract-mediated Ag-doped graphitic carbon nitride (Ag GCN) for photocatalytic degradation of dyes, Environ. Sci. Pollut. Res., **30**, 25650–25662 (2023). doi.org/10.1007/s11356-023-25359-0.

12. P. Parthipan, L. Cheng, A. Rajasekar, M. Govarthanan, and A. Subramanian, Biologically reduced graphene oxide as a green and easily available photocatalyst for degradation of organic dyes, Environ. Res., **196**, (2021). doi: 10.1016/j.envres.2021.110983.

13. J. Gogoi, A.D. Choudhury and D. Chowdhury, Graphene oxide clay nanocomposite as an efficient photo-catalyst for degradation of cationic dye, Mater. Chem. Phys., **232**, 438–445 (2019). doi: 10.1016/j.matchemphys.2019.05.010.

14. X. Jin, N. Li, X. Weng, C. Li, and Z. Chen, Green reduction of graphene oxide using eucalyptus leaf extract and its application to remove dye. Chemosphere., **208**, 417–424 (2018). doi: 10.1016/j.chemosphere.2018.05.199.

15. L. Yuan, W. Liu, and W. Zhang, Potassium-doped g-C_3N_4 enables efficient visible-light-driven dye degradation, Environ. Sci. Pollut. Res., **30**(20), 58276–58281 (2023). doi:10.1007/s11356-023-26520-5.

16. C.Y. Kuo, C.H. Wu, J. T. Wu, and Y. R. Chen. Synthesis and characterization of a phosphorus-doped TiO_2 immobilized bed for the photodegradation of bisphenol A under UV and sunlight irradiation, React. Kinet. Mech. Catal., **114** (2), 753-766 (2014). doi.org/10.1007/s11144-014-0783-2.

17. T. H. Pham, N.M. Viet, P.T. Hoai, S. H. Jung, and T. Kim, Graphitic carbon nitride metal-free photocatalyst for the simultaneous removal of emerging pharmaceutical pollutants in wastewater, Environ. Res., **231**, (2023). doi: 10.1016/j.envres.2023.116246.

18. S. A. Al-Zahrani,M. B. Patil, S. N. Mathad, A. Y. Patil, A. Al Otaibi, N. Masood, D. Mansour, A. Khan, V. Gupta, N. S. Topare, A. Somya and M. Ayyar. Photocatalytic azo dye degradation using graphite carbon nitride photocatalyst and UV-A irradiation. Crystals, **13**(4), 577, (2023). doi.org/10.3390/cryst13040577.

19. S. K. Ben, S. Gupta, A. K. Harit, K. K. Raj and V. Chandra. Enhanced photocatalytic degradation of reactive red 120 dye under solar light using $BiPO_4$-g-C_3N_4 nanocomposite photocatalyst, Environ. Sci. Pollut. Res., **29**(56), 84325–84344 (2022). doi:10.1007/s11356-022-21675-z.

20. I. Dobrosz-Gomez, M.A. Gomez-Garcia, S.M. Zamora, E. Pavas, and J. Bojarska, Transition metal loaded TiO_2 for phenol photo-degradation, **18**,1170–1182 (2015). doi:10.1016/j.crci.2015.03.006.

21. M. Lei, N. Wang, L. Zhu, Q. Zhou, and G. Nie. Environmental Photocatalytic reductive degradation of polybrominated diphenyl ethers on CuO/TiO_2 nanocomposites: a mechanism based on the switching of photocatalytic reduction potential being controlled by the valence state of copper. Appl. Catal. B: Environ. **182**,414–423 (2016). doi.org/10.1016/j.apcatb.2015.09.031.

22. J. Xie, Z. Zhou, Y. Lian, Y. Hao, and P. Li, Synthesis of α-Fe_2O_3/ZnO composites for photocatalytic degradation of pentachlorophenol under UV–vis light irradiation, Ceram. Int., **41**, 2622–2625 (2015). doi:10.1016/j.ceramint.2014.10.043.

23. E. D. Sherly, J.J. Vijaya, and L.J. Kennedy, Visible-light-induced photocatalytic performances of ZnO–CuO nanocomposites for degradation of 2,4-dichlorophenol, Chinese J. Catal., **36**, 1263–1272 (2015). doi:10.1016/S1872-2067(15)60886-5.

24. K. Vignesh, A. Suganthi, M. Rajarajan, and S.A. Sara, Photocatalytic activity of AgI sensitized ZnO nanoparticles under visible light irradiation, Powder Technol., **224**, 331–337 (2012). doi:10.1016/j.powtec.2012.03.015.

25. K. Vignesh, R. Hariharan, M. Rajarajan,and A. Suganthi. Visible light assisted photo catalytic activity of TiO_2-metal vanadate (M = Sr, Ag and Cd) nanocomposites, Mater. Sci. Semicond. Proc., **16**,1521–1530 (2013). doi:10.1016/j.mssp.2013.04.025.

26. C. Karunakaran and S. Senthilvelan, Photocatalysis with ZrO_2: Oxidation of aniline, J. Mol. Catal. A Chem., **233**, (2005). doi:10.1016/j.molcata.2005.01.038.

27. K. Vinodgopal, I. Bedja, and P.V. Kamat, Nanostructured semiconductor films for photocatalysis: Photoelectrochemical behavior of SnO_2/TiO_2 composite systems and its role in photocatalytic degradation of a textile azo dye, Chem. Mater., **8**, 2180-2187 (1996a). doi: 10.1021/es00003a037.

28. M.E. Fabiyi and R.L. Skelton, Photocatalytic mineralization of methylene blue using buoyant TiO_2-coated polystyrene beads, J. Photochem. Photobiol. A Chem., **132**, 121-128 (2000). doi.org/10.1016/S1010-6030(99)00250-6.

29. G. Sivalingam, K. Nagaveni, M.S. Hegde, and G. Madras. Photocatalytic degradation of various dyes by combustion synthesized nano anatase TiO_2, Appl. Catal. B Environ., **45**, 23-38 (2003).

30. Y. Tan, Z. Shu, J. Zhou, T. Li, W. Wang, and Z. Zhao, One-step synthesis of nanostructured g-C_3N_4/Tio_2 composite for highly enhanced visible-light photocatalytic H_2 evolution, Appl. Catal. B: Environ., **230**, 260–268 (2018).

31. Y. Zeng, X. Liu, C. Liu, L. Wang, S. Luo, and Y. Pei. Scalable One-step production of porous oxygen-doped g-C_3N_4 nanorods with effective electron separation for excellent visible-light photocatalytic activity, Appl. Catal. B: Environ., **224**, (2018). doi: 10.1016/j.apcatb.2017.10.042.

32. C. Li, Z. Sun, Y. Xue, G. Yao, and S. Zheng, A facile synthesis of g-C_3N_4/TiO_2 hybrid photocatalysts by sol–gel method and its enhanced photodegradation towards methylene blue under visible light, Adv. Powder Tech., **27**(2), 330–337 (2016).

33. K.C. Christoforidis, T. Montini, E. Bontempi, S. Zafeiratos, J. Jaén, and P. Fornasiero, Synthesis and photocatalytic application of visible-light active β -

Fe_2O_3 /g-C_3N_4 hybrid nanocomposites, Appl. Catal. B: Environ.,**187**, 171–180 (2016).

34. J. Hong, X. Xia, Y. Wang, and R. Xu. Mesoporous carbon nitride with in situ sulfur doping for enhanced photocatalytic hydrogen evolution from water under Visible light, J. Mater. Chem., **22**(30), (2012).
35. C. Bian, Y. Wang, Y. Yi, S. Shao, P. Sun, and X. Dong, Enhanced photocatalytic activity of S-doped graphitic carbon nitride hollow microspheres: Synergistic effect, high-concentration antibiotic elimination and antibacterial behavior, J. Colloid Interface Sci., **643**, 256–266 (2023). doi: 10.1016/j.jcis.2023.04.034.
36. Q. Gao, Q. Lei, R. Miao, M. Gao, and H. Liu, Bi-doped graphitic carbon nitride nanotubes boost the photocatalytic degradation of rhodamine B, New J. Chem., **46**(8), 3588–3594 (2022).
37. Y. Xie, J. Wu, C. Sun, Y. Ling, S. Li, and J. Zhao. La_2O_3-modified graphite carbon nitride achieving the enhanced photocatalytic degradation of different organic pollutants under visible light irradiation, Mater. Chem. Phys., **246**, (2020). doi: 10.1016/j.matchemphys.2020.122846.
38. N. A. Hadadi, U. Baig, M. A. Gondal, M. J. and S. Mohamed, Pulsed laser induced synthesis of graphitic carbon nitride-cadmium selenide nanocomposite for photo-catalytic degradation of organic dyes, and electro-catalytic hydrogen evolution reaction, Colloids and Surf. A: Physicochem. Eng. Asp., **658**, (2023). doi: 10.1016/j.colsurfa.2022.130711.
39. M.-L. Chen, S.-S. Li, L. Wen, and Z. Xu, Exploration of double Z-type ternary composite long-afterglow/graphitic carbon nitride metal–organic framework for photocatalytic degradation of methylene blue, J. Colloid and Interface Sci., **629**, 409–421 (2023). doi: 10.1016/j.jcis.2022.08.189.
40. A. Ahmed, R. Alabada, M. Usman, A. A. Alothman, M. K. Tufail, and S. Mohammad, Synthesis of visible-light-responsive lanthanum-doped copper ferrite/graphitic carbon nitride composites for the photocatalytic degradation of toxic organic pollutants, Diam. Relat. Mater., **141**, (2024). doi: 10.1016/j.diamond.2023.110630.

41. F. Sousani, S.K. Sadrnezhaad, P. Abachi, and H. Mahtabpour, $Ni_{0.8}Co_{0.2}/Zn_{0.8}Cd_{0.2}$ S/g-C_3N_4 ternary nano-photocatalyst for improved visible-light-driven photocatalytic H_2 evolution and pollutants degradation, Int. J. Hydrog. Energy, **51**, 281–299 (2024).

42. M. S. Nivetha, N. Abirami, and R. Arulmozhi, A novel g-C_3N_4@biTiO_2/NIO ternary heterostructure photocatalysts for effective degradation of tetracycline under light illumination, Inorg. Chem. Commun., **159**, (2024). doi: 10.1016/j.inoche.2023.111778.

43. P. Kumawat, M. Joshi, R. Ameta, and S. C. Ameta, Photocatalytic degradation of basic fuchsim over quaternary oxide iron zinc cuprate ($FeZn_2Cu_3O_{6.5}$), Adv. Appl. Sci. Res., **6**(7), 209–215 (2015).

44. H. Abbasi-Asl, M.M. Sabzehmeidani, M. Ghaedi, and Z. Moradi, Bifunctional quaternary magnetic composite as efficient heterojunctions photocatalyst for simultaneous photocatalytic visible light degradation of dye and herbicide pollutants from water and bacterial disinfection, J. Environ. Manage., **345**, (2023). doi: 10.1016/j.jenvman.2023.118656.

45. Akhundi, and A. Habibi-Yangjeh, High performance magnetically recoverable G-$C_3N_4/Fe_3O_4/Ag/Ag_2SO_3$ plasmonic photocatalyst for enhanced photocatalytic degradation of water pollutants, Adv. Powder Technol., **28**(2), 565–574 (2017). doi: 10.1016/j.apt.2016.10.025.

46. M. Qarajehdaghi, A. Mehrizad, P. Gharbani, and G.H. Shahverdizadeh, Quaternary composite of CdS/G-C_3N_4/RGO/CMC as a susceptible visible-light photocatalyst for effective abatement of ciprofloxacin: Optimization and modeling of the process by RSM and ann, Proc. Safety Environ. Prot., **169**, 352–362 (2023). doi: 10.1016/j.psep.2022.11.030.

47. H. P. Gogoi, G. Bisoi, P. Barman, A. Dehingia, S. Das, and A. P. Chowdhury, Highly efficient and recyclable Quaternary Ag/Ag_3PO_4–BiOBr–C_3N_4 composite fabrication for efficient solar-driven photocatalytic performance for anionic pollutant in an aqueous medium and mechanism insights, Optic. Mater., **138**, (2023). doi: 10.1016/j.optmat.2023.113712.

48. V. Hasija, A. Sudhaik, P. Raizada, A. Hosseini-Bandegharaei, and P. Singh, Carbon quantum dots supported AgI /ZnO/phosphorus doped graphitic carbon nitride as Z-scheme photocatalyst for efficient photodegradation of 2, 4-dinitrophenol. J. Environ. Chem. Eng., **7**(4), (2019). doi: 10.1016/j.jece.2019.103272 .

49. A. Kumar, G. Sharma, Mu. Naushad, A.A. Ghfar, and F.J. Stadler, Quaternary magnetic biocl/g-C_3N_4/Cu_2O/Fe_3O_4 nano-junction for visible light and solar powered degradation of sulfamethoxazole from aqueous environment, J. Chem. Eng., **334**, 462–478 (2018). doi: 10.1016/j.cej.2017.10.049.

50. M. Mousavi, A. Habibi-Yangjeh, and M. Abitorabi, Fabrication of novel magnetically separable nanocomposites using graphitic carbon nitride, silver phosphate and silver chloride and their applications in photocatalytic removal of different pollutants using visible-light irradiation, J. Colloid. Inter. Sci., **480,** 218–231 (2016).

51. L. Wang, Y. Li, and P. Han, Electrospinning preparation of g-C_3N_4/Nb_2O_5 nanofibers heterojunction for enhanced photocatalytic degradation of organic pollutants in water, Sci. Rep., **11**, 22950 (2021). doi. org/10.1038/s41598-021-02161-x.

52. R.S. Sahu, Y.-H. Shih, and W.-L. Chen, New insights of metal free 2D graphitic carbon nitride for photocatalytic degradation of bisphenol A, J. Hazard. Mater., **402**, (2021). doi: 10.1016/j.jhazmat.2020.123509.

53. J. Guo, Y. Sun, R. Xiang, H. Xiang, Z. Chen, F. Zhang, and F. Liu, One-step synthesis of porous thin-layered graphitic carbon nitride for enhanced photocatalytic dye degradation, Colloids Surf. A Physicochem. Eng. Asp. Colloid Surface A., **671**, 131600 (2023). doi.org/10.1016/j.colsurfa.2023.131600.

54. S. Habib, M. Serwar, H. M. Siddiqi, U. A. Rana, F. Liaqat, and A. Shabbir, A photocatalytic dye-degradation study on methylene blue by graphitic nitride-based polyimides synthesized via a facile thermal-condensation approach, J. Environ. Chem. Eng., **10**(3), (2022). doi: 10.1016/j.jece.2022.107747.

55. D. Lyu, G. Yu, W. Cao, and C. Hu, Efficient destruction of pollutants in water by a dual-reaction-center fenton-like process over carbon nitride compounds-complexed cu (II)-$CuAlO_2$, Environ. Sci. Technol., **52**, 4294–4304 (2018).

56. C. Jin, J. Kang, Z. Li, M. Wang, Z. Wu, and Y. Xie, Enhanced visible light photocatalytic degradation of tetracycline by MoS_2/Ag/g-C_3N_4 Z-scheme composites with peroxymonosulfate, Appl. Surf. Sci., **514**, (2020). doi:10.1016/j.apsusc.2020.146076.

57. R. Li, J. Huang, M. Cai, Z. Xie, Q. Zhang, Y. Liu, and H. Liu, Activation of peroxymonosulfate by Fe doped g-C_4N_4 /graphene under visible light irradiation for trimethoprim degradation, J. Hazard. Mater., **384,** (2020). doi: 10.1016/j.jhazmat.2019.121435.

58. L. Wang, X. Guo, Y. Chen, S. Ai, and H. Ding, Cobalt-doped g-C_3N_4 as a heterogeneous catalyst for photo-assisted activation of peroxymonosulfate for the degradation of organic contaminants, Appl. Surf. Sci., **467–468**, 954–962 (2019).

❐❐❐